First 3D Ultrasound Scanning, Planning, and Execution of CT-free Milling Interventions with a Surgical Robot

Philipp J. Stolka[1], Dominik Henrich[1], Steffen H. Tretbar[2], and Philipp A. Federspil[3]

1: Lehrstuhl für Angewandte Informatik III (Robotik und Eingebettete Systeme) Universität Bayreuth, D-95440 Bayreuth, Germany
{philipp.stolka, michel.waringo, dominik.henrich}@uni-bayreuth.de

2: Fraunhofer Institut für Biomedizinische Technik (Department Ultrasound); D-66386 St. Ingbert, Germany
steffen.tretbar@ibmt.fraunhofer.de

3: Universitäts-Hals-Nasen-Ohrenklinik Heidelberg D-69120 Heidelberg, Germany
federspil@med.uni-heidelberg.de

Abstract – Surgical procedures with navigation or robot system support usually require pre-operative planning data. This data can be acquired with imaging techniques such as computed tomography (CT), the current gold standard due to its high precision. With such planning data, access trajectories, implant positions, individual milling paths etc. can be computed. We present a novel ultrasound-based method to generate equivalent 3D image data which is well-suited for many interventions, but less costly than the CT-based method. The method is demonstrated for robot-based implant bed milling in the lateral skull base, in a complete process consisting of infrared navigation registration, manual ultrasound scan path delineation, path smoothing and checking, robot-based ultrasound scan execution, 3D ultrasound volume reconstruction, implant position optimization, robot milling path planning, and intervention execution. This represents, to the best of our knowledge, the first time such a CT-free, 3D-ultrasound-based intervention has been demonstrated in the laboratory.

Keywords: ***surgical robotics, 3D ultrasound, navigation, planning, implant optimization, milling***

I. Introduction

Performing surgical procedures with the assistance of navigation or robotic systems usually consists of several pre-operative steps during the preparation phase (imaging and planning) and several intra-operative steps during the execution phase (registration and actual plan execution). Such computer- or robot-assisted surgery (*CAS/RAS*) systems only fully exhibit their benefits when operating on high resolution imaging data and good quality registration, i.e. successful determination of the geometric relationship between planning data and execution site. Traditionally, this is achieved with „gold standard“ procedures, consisting of a computed tomography (*CT*) scan of the patient and inclusion of implanted or temporary artificial markers for registration in the operating room (*OR*). Precision requirements are especially high for surgical robots in orthopedic applications. With appropriate planning data, individual trajectories in optimally determined positions can be computed for the respective milling, drilling, or sawing operations. These need to be retrieved exactly by registration procedures in the OR to fully utilize the positioning precision of robots and the computer-assisted planning.

Addressing the most important drawbacks of this approach (time requirements, radiation exposure, and invasiveness) we present a robot-based 3D ultrasound scanning method to generate intra-operative global image data. The method produces data of equivalent use to that of traditional CT but is less costly and can be used to perform both intervention planning and registration. The patient is not exposed to x-ray radiation, and since the presented method is markerless – it does not rely on (implanted) pins – it can alleviate the need for time-consuming pre-operative preparation and imaging procedures. As imaging is performed just before execution, planning takes place directly in the pre-registered image data without any external registration methods.

The scope of application for the presented system is the automated milling of cavities in the lateral skull bone for subder-

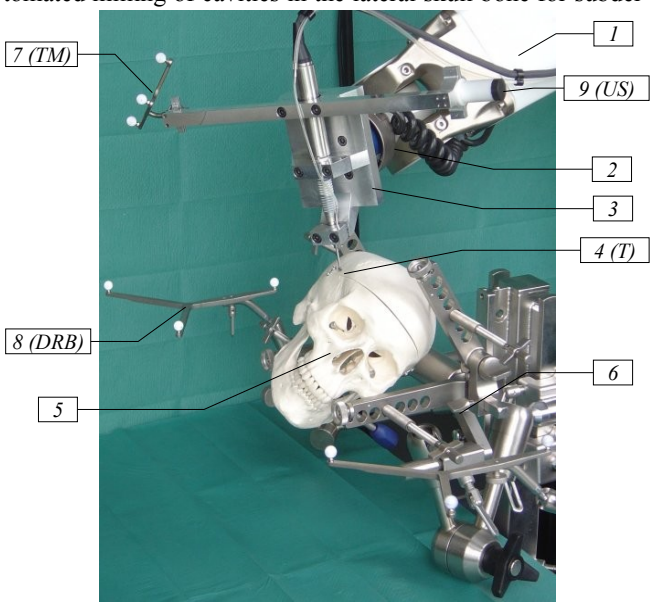

Figure 1: Setup of the RONAF system – robot arm (1) with force/torque (F/T) sensor (2), tool holder (3), surgical miller tip (4), skull phantom (5), fixtures (6), infrared-reflective markers of the tool (7) and the robot base (8), and the A-mode ultrasound sensor (9)

mal implantation of hearing aids, where one process step is the removal of bone material from the thin skull bone (*calotte*) in the shape of flat amplifier components (Figure 9) [6], [7]. Other applications would be *mastoidectomies* (removal of bone volumes behind the ear) or generally any intervention where ultrasound data can effectively replace imaging, e.g. orthopedic knee or hip interventions. In the presented system, the ultrasound planning data serves for implant position optimization and milling path generation. The robot can finally execute the milling without any additional registration.

Based on the state of the art (Section II), one can justify the development of a robot-based 3D ultrasound system (Section III). The implementation (Section IV) is experimentally validated for the whole process on human preparations (Section V). Finally, the outlined conclusions indicate the possible direction of future work (Section VI).

II. State of the art

Currently, the standard imaging modality for planning in autonomous and/or cooperative robot-assisted surgery (*RAS*) systems is global preoperative data from CT, with magnetic resonance imaging (*MRT*) following closely. Examples are the commercial systems Robodoc [10] and CASPAR (orthopedic knee and hip interventions), the AcroBot (knee) [2], or research systems like RobaCKa [3] and CRANIO/CRIGOS (orthopedic interventions on the skull) [1]. They require imaging procedures before the intervention and some means of registering imaging data with the OR situation, e.g. implanted markers.

Alternatives for certain cases include atlas-based image-free methods, e.g. by sampling bone surface regions or pivot points with hand-held pointers, fitting a model to patient-specific features (e.g. „BrainLab VectorVision knee“).

The use of ultrasound (*US*) has been traditionally limited for manual intervention planning purposes due to its low resolution. However, its non-invasive nature makes it a preferable choice for registration, as with tracked US A-mode (i.e. 1D) probes to register the patient with a prior CT scan, e.g. [16]. However, recent developments towards high-precision US systems enable their use at least for situations where the thickness of tissues with highly different densities needs to be measured [4], [5], [12].

However, actual 3D ultrasound scanning for planning and registration can be found in only a small number of projects, e.g. in the IR-navigated B-mode (2D) manual scanning of the shoulder/elbow area with concurrent 3D volume reconstruction in [8]. As the resolution and precision of conventional US probes is low, this data is difficult to use for planning CAS/RAS interventions.

Together, the combination of robot-based interventions with 3D ultrasound as the basis for planning (instead of CT) has not been presented in the literature, in spite of its potential advantages, such as non-invasiveness of imaging and registration, no radiation exposure, and potential high axial resolution.

III. Registration and Surface Scanning

Therefore, we can state our design requirements as follows: Discarding CT in favor of US imaging for orthopedic interventions makes high-precision measurements necessary, with distance and preferably bone thickness being sampled with a precision comparable to the ca. 0.4 mm standard set by conventional CT. Furthermore, because the US probe does not provide global positioning information we need a means of locating the samples relative to each other with a spatial and temporal precision resulting in volume reconstruction better than or comparable to CT. Finally, the volume needs to be *registered* to the robot precisely enough to be useful for navigation, i.e. the transformation from planning data to the robot coordinate system must be established.

With the presented method, several implicitly registered image modalities are generated for navigation. To achieve this, several transformations – between the robot, optical tracking system, and IR pointers – need to be established first (Section A). Then, a skull surface representation is manually sampled with a hand-held pointer. Robot-based scanning relies on a manually defined path that has to be smoothed (Section B) before further processing (Section C). Path planning for the robot may bring about kinematic problems that need to be addressed before actual execution (Section D). Scanning the skull returns both outer and inner skull boundaries. Sampling the two strongest echoes with a robot-held A-mode US probe yields two sets of positions which enter the 3D ultrasound volume reconstruction (Section E). This allows to compute an optimal implant position (Section F) and milling paths (Section G) to finally perform the milling intervention (Section H) without additional registration.

A. Registration of Robot, Optical Tracking, and Pointers

The registration relationships between the robot, optical tracking system (*OTS*), hand-held pointers, skull surface, and the US scan path for the presented system are shown in Figure 2. The rigid tool combination including miller and US probe forms one registration entity which needs to be registered to the actual patient in the operating room (*OR*). Since imaging data originates directly from the current patient situation, patient and bone representation can be identified as one entity without additional registration procedures. The milling volume later needs to be positioned within this representation.

First, the robot performs motions to calibrate the milling tool and its rigidly attached IR marker and register both in OTS coordinates (Objects 4 and 7 in Figure 1).

Second, the user calibrates a hand-held OTS pointer and samples a skull surface points representation by sliding the pointer over the exposed skull, which is already registered with the robot by now.

Third, the pointer is used to define the 3D positions making up the scan path on the skull surface to be followed by the robot-held US probe (Figure 3). We allow the user to perform this step manually to allow explicit consideration or omission of problematic regions with strong curvature or sensitive structures.

For suitable, lattice-like scan paths with neighboring passes at a distance of ~10mm over an area of ~$(50\text{mm})^2$, this results in a scan path length of ~600mm. Now the 3D points acquired must be processed before path execution by smoothing and surface normal determination procedures.

B. Scan Path Smoothing

In order to speed up scanning, the scan path is straightened by successively removing points until the resulting path devia-

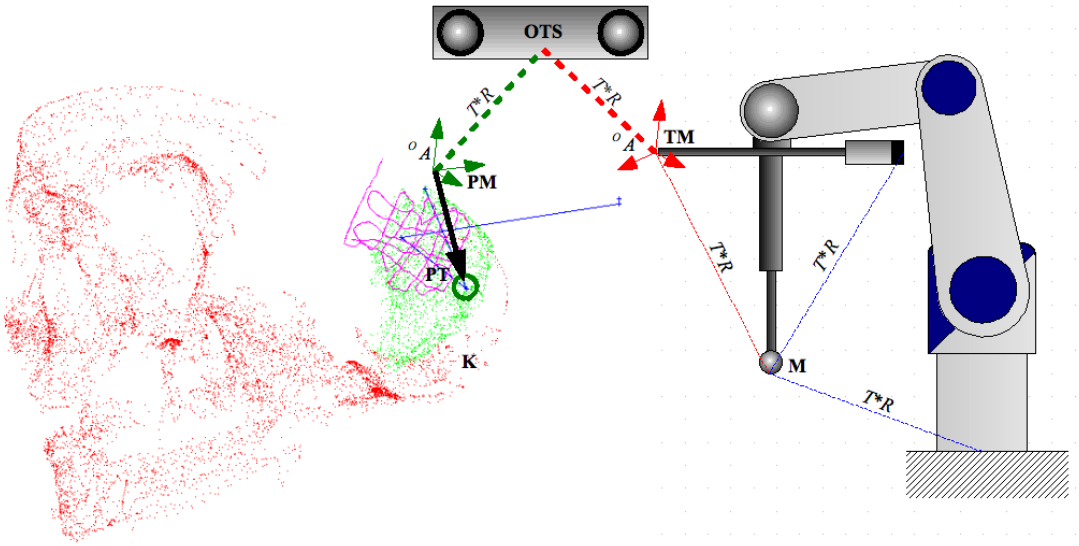

Figure 2: Registration (translations T, rotations R) between robot, tool and US probe (tool tip M, tool infrared marker TM), the optical tracking system (OTS), and scan path (K) demonstrated by a hand-held pointer (tip PT, marker PM)

tion exceeds an application-specific threshold. The algorithm for removing path points is described in detail in [15]. Figure 4 shows an initial US scan path and the result of path straightening.

This runtime of this step is on the order of a few seconds.

C. Surface Normals Determination

The US probe needs to be oriented almost perfectly perpendicular to the scanned surface in order to receive satisfying US echoes later, especially for inner boundary samples.

In the next step, surface normals over a local sample neighborhood are determined from the scan path and surface points which approximate a possibly non-planar surface. We need the point m (taken from the scan path) for which the normal vector should be determined. It is not required for m to be contained in the surface defined by the point cloud, although ideally it should be close to it.

The algorithm (described in [18]) can be subdivided into three steps. First, the space P containing all the points is hashed allowing for fast access to neighboring points. The next two steps consist of finding a subset of relevant points $n_i \in Q \subseteq P$ in the proximity of m and computing the normal vector on the surface approximately defined by Q. These steps are repeated for each normal vector (Figure 5).

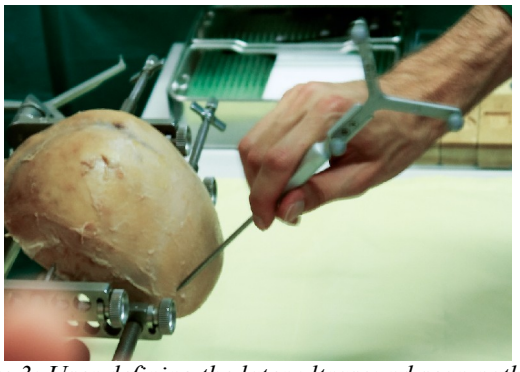

Figure 3: User defining the later ultrasound scan path with a handheld IR pointer

Effective calculation times are ca. 1 min for the data sets encountered in the experiments.

D. Robot-Based Ultrasound Scan Execution

The procedure described so far yields a sequence of 3D positions with two rotational degrees of freedom (*DOF*) fixed. This leaves each one DOF open for each point; in the presented system this is the rotation around the long tool axis („roll"). Since the US probe operates in A-mode, each shot is rotationally invariant around this DOF, which can therefore be set to any kinematically valid value between 0° and 360°.

By arbitrarily selecting one orientation around the US sensor axis, the scan path can be followed, guiding the probe perpendicularly to the skull surface. However, in the presented case, the robot has six non-redundant DOF, and following the the skull's curvature with the robot-held probe often leads to kinematic problems, resulting in path abortion. Therefore, after registration of the robot, the patient, and the 5D path, a valid 6D path is searched from a set of paths generated with different roll values that are held constant over the whole path [18]. In the current implementation, the first completely traversable path is selected for execution. If no kinematically admissible path is found, the robot base location must be changed.

The final scan path execution with concurrent ultrasound sampling (Figure 6) returns a sequence of US A-scans, with the single upper and lower skull boundaries detectable by

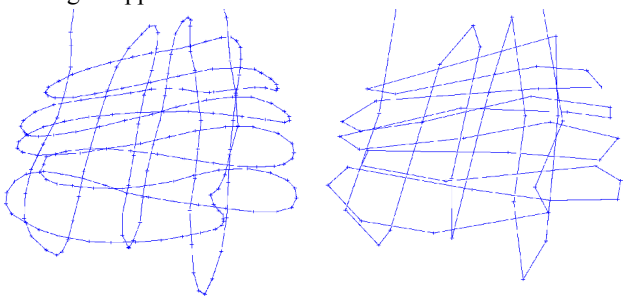

Figure 4: An ultrasound scan path on a human skull – original (left, 307 points), straightened path (right, 90 points)

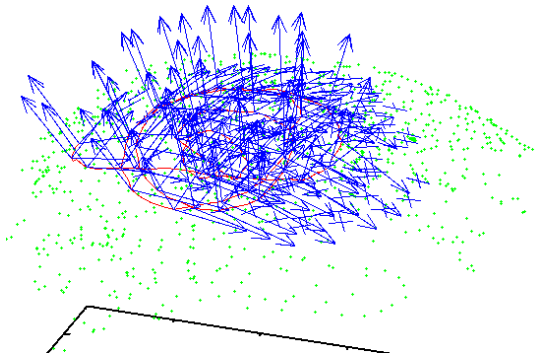

Figure 5: Surface points (green), US scan path (red; both sampled with IR pointer), and computed robot orientations (blue) for roll angle –20°

thresholding the filtered radio-frequency signal. For better results, matched filtering is performed with coded excitation chirp signals. Instead of single ultrasound pings, a modulated waveform is emitted and cross-correlated with its echoes, improving detection in spite of a low signal-to-noise ratio [12].

To ensure stable contact between US probe and skull even when the initial scan path definition is faulty due to calibration errors, the scanning is performed under force-based pressure control. To achieve this, the robot is subjected to a position P-law control with force target value F_{target} = 15 N along the sensor Z axis upon contact. The resulting deviations relative to the initial scan path do not show up in the echo positions – they are effectively cancelled out by the smaller US delay line thickness when compressed (up to the measurement error; Figure 8).

For the described lattice-like scan path and a robot scan speed of ca. 5 mm/s, the full force-controlled scan takes around two minutes.

E. 3D Ultrasound Volume Reconstruction

In the next step, both boundaries are combined into one cloud and serve to create a non-convex hull with the Powercrust algorithm [19] (Figure 7; it should be noted that the existing noise of the lower boundary extends the hull downwards). Once this is achieved, the hull's surface representation is rastered into a voxelspace and filled up to create the skull bone volume. This whole process results in data structures still registered with the patient in robot coordinates.The runtime of these steps is negligible.

Figure 6: The robot executing the previously demonstrated, post-processed ultrasound scan path on a human specimen.

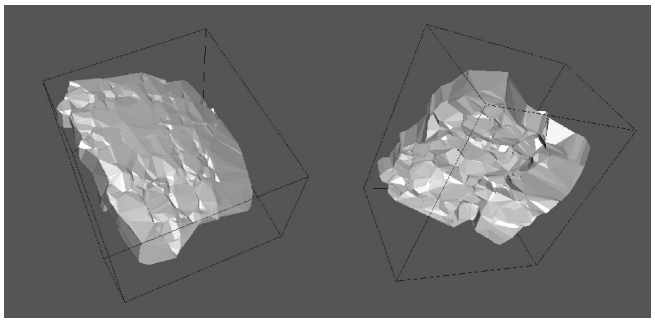

Figure 7: 3D ultrasound surface (left: seen from above, right: below; reconstructed with Powercrust algorithm)

F. Implant Position Optimization

The implant now needs to be positioned within the reconstructed volume. In spite of the limited size of the scanned region and functional constraints on suitable implant positions, determining a reasonably good 6D transformation to position the implant is non-trivial [13]. One investigated optimization criterion is the proximity of points on the implants upper side to the upper bone profile, i.e. how well it blends into the skull surface. One constraint is to accept only small transgressions of the lower profile, i.e. to prevent breaking through the skull. This results in positions mostly oriented along the upper boundary (Figure 10). The quality of the lower boundary points (as described in the previous section) might be a problem for very thin bones; for future work it might become necessary to adapt this constraint criterion respecting the stochastical nature of the lower profile.

Depending on convergence criteria and optimization parameters (number of optimization points etc.), the runtime of this step is on the order of less than one minute.

G. Milling Path Planning

Having determined the implant position within the bone volume, the last planning step is the computation of corresponding milling paths [14]. These are determined in the voxel representation and can be either generic (pre-computable, Figure 9) or individual (with shorter path length based on reaming out only the intersection volume). Furthermore, it is advisable to compute aggressive paths, i.e. such that ream out at least the intersection volume – this is non-trivial due to the spherical miller head shape. Current work concentrates on optimization of the miller inclination based on achievable feed rates and other criteria.

H. Milling Intervention Execution

For the robot-based milling intervention the path executability is tested (similarly to the ultrasound scan paths) before launch. The milling itself is force-controlled to keep thermal trauma to the bone at a minimum [6].

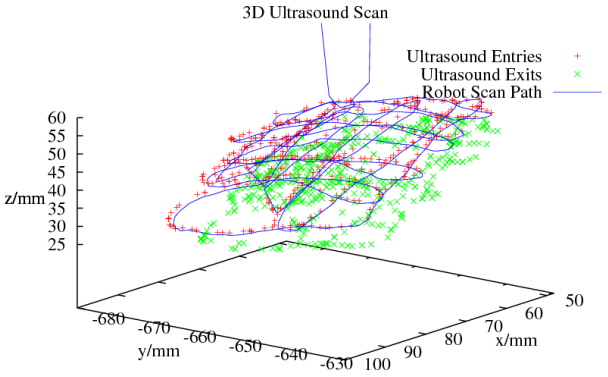

Figure 8: The executed scan path (blue line) and the resulting outer (red) and inner (green) ultrasound samples

Milling duration is about 2...5 min, depending on miller size, force-based speed control effects, and the sinking depth of the implant-bone intersection volume (Figure 11).

IV. Application and System

The validity of the presented method was tested on a system used for automated milling of cavities in the shape of hearing aid amplifier components (Figure 9) from the skull bone. The RONAF project (*Robot-based Navigation for Milling at the Lateral Skull Base*, [6]) examines various navigation methods in autonomous surgical robotics.

The robot is an industrial model (Stäubli RX90) for medical use in hip and knee endoprosthesis milling applications (CASPAR, by Orto-Maquet). Sensors include – amongst others – a 6D force/torque (*F/T*) sensor (JR3 90M31A), an NDI Polaris infrared-optical tracking system (*OTS*; measured repeatability accuracy 0.05 mm root-mean-square (*RMS*), absolute accuracy 0.35 mm RMS, silo-shaped work volume ca. (1000 mm)³, data rate 20...60 Hz), and a Transmit-Receive Module II ultrasound probe (*US*; by Fraunhofer IBMT, St. Ingbert/Germany). The US system control computer is connected with the robot for position acquisition via a local network. Using an ultrasound probe (center frequency 1 MHz, diameter ½ in.) with a flexible delay line, filtered and unfiltered radio frequency signals are available for signal processing. The tool is a surgical miller (electric; Aesculap microtron EC/GD622, up to 30,000 rpm) mounted perpendicularly to the robot tool flange to minimize deformation (Figure 1, [9]).

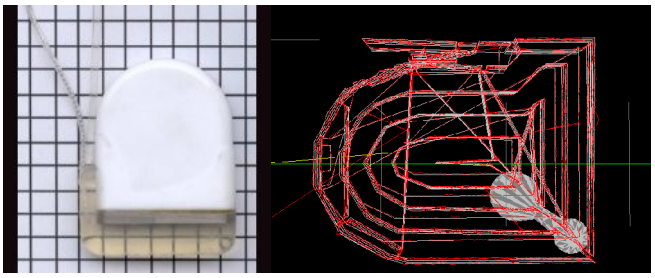

Figure 9: Combi40+ implant (left); milling path (right; shown in grey; red overlay: estimations of miller head positions during bone milling based on force measurements [9])

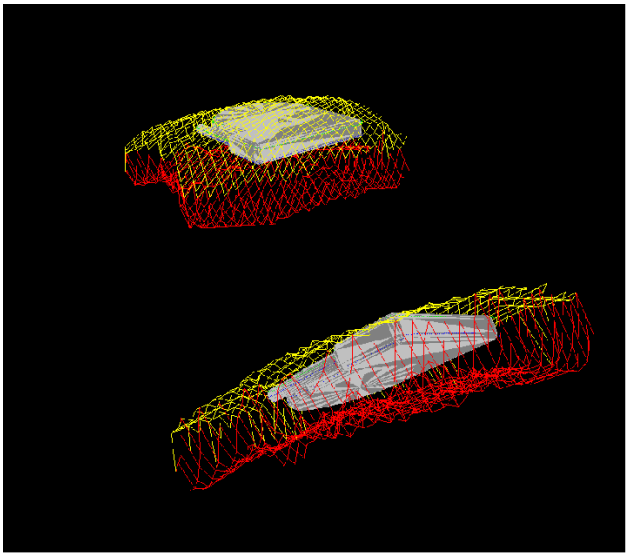

Figure 10: Implant geometry (Combi40+) optimized into 3D ultrasound reconstruction. Note how the implant top approximates the upper skull boundary.

V. Experiments and Results

We performed the described procedure, including pointer and robot calibration and registration, sampling of skull surface points, demonstration and processing of scan paths, and their execution with concurrent US scanning, on five human skull preparations and one plastic skull dummy. Planning and milling was then performed in two human preparations and the dummy.

The manually generated surface point cloud is a 2.5D global map registered to the robot with a precision of <2.5 mm RMS. A precise discussion of the definition and a measurement of this cumulative error can be found in [9]. Low registration quality in this step sometimes resulted in scan paths off the actual skull surface. However, with the flexible delay line attached to the front of the US probe and force-based contact pressure control, all scans could be completed successfully. Especially the latter control proved very useful. The relative number of measureable ultrasound thicknesses went up (to ca. 75 %), and in these the signal strength, especially of the second (inner) echo, increased.

The US scan generates two 2.5D skull surface point clouds which are registered to the robot with a precision determined by and equal to the robot's absolute positioning accuracy (which in turn is close to its relative accuracy of ca. 0.35 mm in local neighborhoods). Another factor in the scan map's pre-

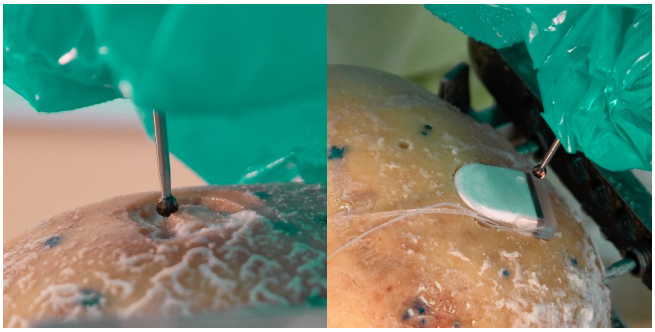

Figure 11: Robot-based milling of the implant bed. The implant fits into the cavity within very tight limits.

cision is the accuracy of thickness detection in the single US shots, which is ca. 0.5 mm (standard deviation for US pulse code excitation with direct coupling of transducer and bone [17]).

The upper profile points correspond to the path actually traversed by the US sensor's calibrated delay line edge up to a precision of ca. 0.1 mm, i.e. well within the robot's positioning accuracy. The lower profile points' precision is less easy to estimate. The only ground truth not introducing additional positioning errors apart from its own resultion is a CT of the region of interest, registered to the 3D ultrasound volume. Initial comparions resulted in deviations of the lower profile relative to the the CT of around ca. 0.7 mm.

Since implant position planning takes place in the reconstructed US volume in an essentially continuous fashion, and the resulting position is transferred to the robot in a floating point format, there are no errors introduced here.

Milling the implant cavity in the bone introduces errors through the robot's tool positioning, tool interaction (cutting/tearing bone), and deformations under load. The latter have been determined in earlier experiments [9] to stay well below ca. 1.75 mm for the force range dictated by physiology and permitted by the force-based speed control. The final implant bed fits the implant to within ca. 1 mm around its edges, and no breakthroughs occurred. This precision is expected to be sufficient for complication-free healing.

VI. Conclusions

We have described a process for bone surface and ultrasound scan path input using an IR pointer registered with a robot, resulting in a navigation system-based surface map and a robot-based 3D ultrasound map with extracted skull boundaries. These maps are registered non-invasively, thus representing an advance in RAS planning data acquisition. Moreover, our results show the feasibility of planning and executing robot-based cochlea implant bed preparations in the skull without either prior CT imaging or any additional registration procedures, representing a big step forward in image-based surgery.

With respect to the initial design requirements, we can state that the 3D ultrasound and surface maps created can be used for CT-free interventions. Bone thickness can be measured with a precision of 0.5mm, comparable to CT. These measurements are compiled into a reconstruction volume based on the spatial information supplied by robot encoders, resulting in a maximum expected ~0.35mm imprecision in the position of the reconstruction, *including* registration error between reconstruction and robot. First results with the 3D US volume reconstruction itself (robot-based or manual) compared to CT have shown the precision to be within an ~0.7mm error. The overall precision of the complete intervention is sufficient to safely place an implant into the thin skull bone at the planned position.

It might be possible to adapt the presented procedure and algorithms to other milling interventions. One example could be the transcutaneous 3D ultrasound acquisition of the femur for hip endoprosthesis implantations, maybe supported by X-ray images to help the surgeon judge the expected bone density before planning the implant position, but otherwise making marker implantation or CT acquisition obsolete.

Acknowledgements

This work is a result of the project „Robot-based navigation for milling at the lateral skull base (RONAF)“ of the special research cluster „Medical navigation and robotics“ (SPP 1124) of the Deutsche Forschungsgemeinschaft (DFG), performed in cooperation with the Universitäts-HNO-Klinik (Abt. HNO-Heilkunde) in Heidelberg/Germany. Further information can be found at *http://ai3.inf.uni-bayreuth.de/projects/ronaf/*.

References

[1] G. Brandt, K. Radermacher, A. Zimolong, G. Rau, P. Merloz, T.V.S. Klos, J. Robb, H.W. Staudte, *“CRIGOS - Entwicklung eines Kompaktrobotersystems für die bildgeführte orthopädische Chirurgie”*, Orthopädie 2000 - 29:645-649, Springer-Verlag 2000.

[2] B.L. Davies, S.J. Harris, W.J. Lin, R.D. Hibberd, R. Middleton, J.C. Cobb, *“Active Compliance in robotic surgery – the use of force control as a dynamic constraint”*, Proc. Instn Mech Engrs, Part H, Journal of Engineering Medicine 211(4), 1997.

[3] D. Engel, J. Raczkowski, H. Wörn, *“RobaCKa: Ein Robotersystem für den Einsatz in der Chirurgie”*, Proc. Workshop 'Rechner- und sensorgestützte Chirurgie', eds. Wörn et al, Heidelberg 2001.

[4] P.A. Federspil, S.H. Tretbar, P.K. Plinkert, “*Increase the Accuracy in Navigated Surgery by in site Measurement of individual Sound Velocity in Skull Bone*”, CURAC'05, Berlin/Germany, Sept 2005.

[5] P.A. Federspil, S.H. Tretbar, C. Sittel, P.K. Plinkert, “*SonoPointer® - a prototype system for ultrasound scanning of skull bone thickness*”, AORL 2006 (in Press).

[6] D. Henrich, “*Robotergestütztes Fräsen an der lateralen Schädelbasis: Kraft-basierte lokale Navigation bei der Implantatbettanlage*”, Robotik 2002, Ludwigsburg/Germany, June 2002.

[7] D. Henrich, Ph. Stolka, “*Principles of Navigation in Surgical Robotics*”, *MRVN 2004*, Remagen/Germany, March 2004.

[8] U. v. Jan, D. Sandkühler, L. Kirsch, H.-M. Overhoff, „*Definition of a humerus coordinate system from semiautomatically segmented 3-D ultrasound volumes*“, Biomedizinische Technik (49) Ergänzungsband, Schiele&Schön, Berlin, 2004.

[9] Ph. Stolka, D. Henrich, „*Improving Navigation Precision of Milling Operations in Surgical Robotics*“, IROS 2006, Beijing/China, 2006.

[10] R.H. Taylor et al, „*An image-directed robotic system for precise orthopaedic surgery*“, IEEE Transactions on Robotics and Automation 10(3):261-275, June 1994.

[12] S. H. Tretbar, Ph.A. Federspil, P.K. Plinkert, “*Improved ultrasound based navigation for robotic drilling at the lateral skull base*”, CARS 2004

[13] M. Waringo, Ph. Stolka, D. Henrich, *“First System for Interactive Position Planning of Implant Components“*, *CURAC 2003*, Nürnberg/Germany, 2003.

[14] M. Waringo, D. Henrich, „*3-Dimensionale schichtweise Bahnplanung für Any-Time-Fräsanwendungen*“, VDI Robotik 2004.

[15] M. Waringo, D. Henrich, „*Efficient Smoothing of Piecewise Linear Paths with Minimal Deviation*“, IROS 2006, Beijing/China, 2006.

[16] S. Winter, B. Brendel, A. Rick, M. Stockheim, K. Schmieder, H. Ermert, „*Registrierung 3-dimensionaler CT- und Ultraschalldaten anhand von Knochenstrukturen*“, 1. Jahrestagung der Deutschen Gesellschaft für Computer- und Roboter-assistierte Radiologie und Chirurgie (CURAC), Leipzig/Germany, 2002.

[17] S.H. Tretbar, Ph.A. Federspil, C. Günther, P.K. Plinkert, *„Ultraschall-Dickenmessung der Schädelkalotte zur Registrierung bei navigierten Eingriffen an der lateralen Schädelbasis“*, Biomedizinische Technik 2004, 49 Ergänzungsband 2 (858-859), 2004.

[18] Ph. Stolka, M. Waringo, D. Henrich, S.H. Tretbar, Ph.A. Federspil, *„Robot-Based 3D Ultrasound Scanning and Registration with Infrared Navigation Support“*, ICRA 2007, Rome/Italy, 2007.

[19] N. Amenta, S. Choi, R.K. Kolluri, *„The Power Crust“*, Proceedings of 6th ACM Symposium on Solid Modeling, 2001, pages 249-260.